Geochemistry Geophysics Geosystems G3
AN ELECTRONIC JOURNAL OF THE EARTH SCIENCES
Published by AGU and the Geochemical Society

Technical Brief
Volume 8, Number 6
6 June 2007
Q06004, doi:10.1029/2007GC001577
ISSN: 1525-2027

Flare imaging with multibeam systems: Data processing for bubble detection at seeps

J. Schneider von Deimling
Leibniz-Institute of Marine Sciences at Kiel University (IFM-GEOMAR), Wischhofstraße 1-3, D-24148 Kiel, Germany (jschneider@ifm-geomar.de)

J. Brockhoff
L-3 Communications, ELAC Nautik GmbH, Neufeldtstraße, D-24118 Kiel, Germany (joerg.brockhoff@elac-nautik.com)

J. Greinert
GNS Science, 1 Fairway Drive, Avalon, P.O. Box 30-368, Lower Hutt, 6315, New Zealand (j.greinert@gns.cri.nz)

[1] Multibeam sonar surveys have been conducted since their invention in the 1970s; however, mainly reflections from the seafloor were considered so far. More recently, water column imaging with multibeam is becoming of increasing interest for fisheries, buoy, mooring, or gas detection in the water column. Using ELAC SEABEAM 1000 data, we propose a technique to detect gas bubbles (flares) although this system is originally not designed to record water column data. The described data processing represents a case study and can be easily adapted to other multibeam systems. Multibeam data sets from the Black Sea and the North Sea show reflections of gas bubbles that form flares in the water column. At least for reasonably intense gas escape the detection of bubbles is feasible. The multibeam technique yields exact determination of the source position and information about the dimension of the gas cloud in the water. Compared to conventional flare imaging by single-beam echo sounders, the wide swath angle of multibeam systems allows the mapping of large areas in much shorter time.

Components: 4067 words, 5 figures, 1 table.

Keywords: multibeam; sonar; flare imaging; bubbles; acoustic, data processing; methane seeps.

Index Terms: 4259 Oceanography: General: Ocean acoustics; 3094 Marine Geology and Geophysics: Instruments and techniques; 3004 Marine Geology and Geophysics: Gas and hydrate systems; 4562 Oceanography: Physical: Topographic/bathymetric interactions.

Received 3 January 2007; **Accepted** 23 January 2007; **Published** 6 June 2007.

Schneider von Deimling, J., J. Brockhoff, and J. Greinert (2007), Flare imaging with multibeam systems: Data processing for bubble detection at seeps, *Geochem. Geophys. Geosyst.*, *8*, Q06004, doi:10.1029/2007GC001577.

1. Introduction

[2] Multibeam sonar technology was developed in the 1970s to map the seafloor more efficiently than with single-beam surveys. Since its first deployment in 1977 (SEABEAM, R/V *Jean Charcot*), systems have improved tremendously with regard to coverage and resolution resulting in a maximum

of 150° opening angle and beam widths of less then 1°.

[3] So far, multibeam applications have mainly been used to gather information about the seafloor; because of computer and data storage limitations water column information could not be recorded in the past.

[4] Bottom detection algorithms (BDA) extract the "valuable" data as water depth and amplitude/backscatter values of the seafloor but at the same time disregard almost any water column information irreversibly.

[5] Meanwhile, today's computer technology allows recording and storing of huge amounts of data and water column imaging (WCI) swath sonars are feasible. The growing interest in WCI with multibeam sonar systems is shown in the increasing implementation of WCI in modern multibeam systems (e.g., ELAC swept beam 3012, Kongsberg Ex-Simrad Raw data Logger, latest Atlas Hydrosweep DS). The field of applications is widespread and covers fisheries [*Mayer et al.*, 2002], buoy, mooring and mine detection as well as the detection of natural bubble releasing seepage [*Schmale et al.*, 2005; *Naudts et al.*, 2006; *Greinert et al.*, 2006].

[6] In the following, we will concentrate on the hydroacoustic detection of natural gas escape (flare imaging), a phenomenon that occurs globally in coastal deposition environments, major deltas, or hydrocarbon-bearing sedimentary basins on the continental shelves and slopes [*Hovland and Judd*, 1988; *Judd and Hovland*, 2007]. Gas seepage is frequently linked to gas hydrate deposits [*Judd et al.*, 2002]. We will present data from a seep area in the Black Sea and a gas well blow-out site in the North Sea. At both sites, gas bubbles of mm to cm size issue from the seafloor are released in 90 to 240 m water depth. We will show that information about the water column can even be obtained using multibeam systems without WCI support. The phenomenon of seafloor masking as well as special processing and 3-D visualization techniques will be described below.

2. Background and Methods

2.1. Interference of Bubbles With Hydroacoustic Systems

[7] The detrimental influence gas bubbles have on the quality of sonar surveys, e.g., as reverberation or damping, is well known. In many cases bubbles are carried into the surface water through breaking waves and the vessel movement itself. If a certain threshold of free gas is reached in the vicinity of the transducers, the transmission of acoustic energy is blocked, which results in a total failure of the sonar system. However, below 10 to 20 m water depth the effect of atmospheric air bubbles can be neglected [*Lurton*, 2002].

[8] The situation is different when bubbles rise from the seafloor. In most cases, the bubbles will not reach the transducer and the transmission of energy into the water will not be disturbed. But since bubbles act as strong reflectors, they can be misinterpreted as bottom signals depending on environmental circumstances and the multibeam system used.

[9] The strong impact of bubbles on acoustic wave propagation is based on the great impedance difference between water and free gas phase. If a bubble is big enough (radius must be considerably bigger then the wavelength), much of the wave energy is backscattered. This is especially true for an ideal sphere since any incident wave will hit the sphere perpendicular to its surface; accordingly, bubbles can be detected in monostatic setups. Bigger bubbles (>1 mm) will not behave like ideal spheres, they are elliptically shaped and expose a larger area toward the incident wave from above [*Clift et al.*, 1978]. At a certain frequency f_{res}, bubbles become resonant depending on bubble size and pressure. In this case the bubble acts as a resonator with part of the energy being damped where the remaining part is transmitted as waves of f_{res} in any direction. The differential backscattering strength toward the transducer reaches a maximum.

[10] For the given frequencies (50 and 180 kHz) and depths (90 to 250 m) of our field data, the critical radii for resonance are smaller than 0.3 mm. Direct bubble size distribution measurements at seeps [*Greinert and Nützel*, 2004; *Leifer and Boles*, 2005] suggest hardly any bubbles <0.5 mm exist. Visual observations in the Black Sea by submersible [*Michaelis et al.*, 2002; *McGinnis et al.*, 2006] confirmed that bubbles are typically several mm in size. Nevertheless, as most rising bubbles from "normally" active seeps will not reach the sea surface [*McGinnis et al.*, 2006] because of dissolution, bubbles should become resonant at a certain depth. If many bubbles are close to each other (closer than the wavelength), multiple backscattering will occur [*Clay and Medwin*, 1977] changing the received signal strength completely.

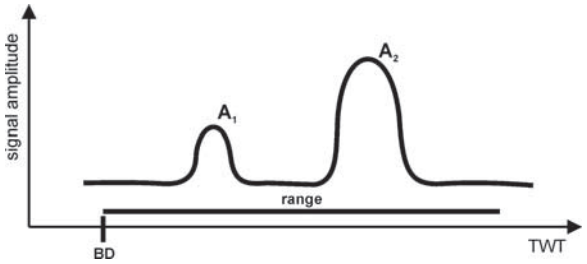

Figure 1. Schematic time series of the envelope of two echo signals, from a bubble cloud (A_1) and the seafloor (A_2). The block depth (BD) and the range determine the relevant time series (TWT is two-way traveltime).

[11] The detection of bubbles with conventional multibeam systems strongly depends on the implemented bottom detection algorithm (BDA), filter routines, data storage capacity apart from a sufficient amount of bubbles in the water. In conventional systems, bubbles appear as bottom signal spikes if the data are not filtered by the system at a very early stage. Particularly the BDA is critical for our purpose as discussed in the following.

2.2. Description of the System Used

[12] The multibeam used was a SEABEAM 1000 [*L-3 Communications ELAC Nautik GmbH*, 2003] with 126 beams, 3 × 1.5° beam angle mounted as 157 or 120° system in the moon pool. On R/V *Poseidon* the system was equipped with 50 kHz transducers (120° swath angle) and on R/V *Alkor* with 180 kHz transducers (157° swath angle). The system was motion compensated by an IXSEA 3000 unit fixed directly above the transducers in the moon pool. This unit also provided heading data. The sound velocity at the transducers was taken from a MiniSVP (Valeport). Positioning was supplied by the ship's GPS.

[13] Data were recorded by the experimental "Water Column Imaging" version of Hydrostar-Online (HSO) by ELAC-Nautik. This version was adapted for IFM-GEOMAR by ELAC-Nautik in 2004 to record the entire signal trace of one of the 42 physically transmitted beams. Usually, the center beam was chosen for recording and for the online display of the water column signal (comparable to a normal single-beam echo sounder). The most critically discriminating parameter between echoes from the seafloor and echoes reflected by bubbles was the quality factor, assigned by the SONAR processing. For a better understanding of this step we provide a more detailed explanation of the BDA below.

[14] In general, the BDA of the SEABEAM 1000 series is designed to retrieve echoes most likely returned from the seafloor and to reject any other echo. Once a sounding is accepted as a feasible seafloor signal, it is assigned a quality flag to provide information about the detection reliability for later data analysis. The signal output from the beam former is the input to the BDA. This amplitude time series contains signals from the seafloor echo as well as echoes from the water column like bubbles or fish (Figure 1). The BDA is implemented as a convolution of a customized response function with the beam formed amplitude time series.

[15] The response function accounts for transmit pulse length and pulse widening with increasing grazing angle. The resulting time series is analyzed for maxima which determine the two-way traveltime, signal amplitude and a quality factor for each beam. If more than one echo (maximum) is received, the BDA selects the most feasible one, which is normally the one with the highest amplitude. Quality factors of 1 to 4 are assigned to each selected signal using the ratio between the second and first strongest signal received in time (Table 1). Quality 4 describes data where this ratio is bigger then 1.

[16] In case of two equally strong returns, the BDA selects the one that fits best to the previously measured beam and assigns a quality of 5. Sometimes the second strongest signal fits considerably better with the previously measured beam and thus is selected as more feasible despite its lower amplitude. The BDA algorithm incorporates a hysteresis to prevent oscillating between two feasible values, comparable to clutter filter often found in RADAR applications. The quality factors assigned in this case are 6 or 7 depending on the ratio between the finally selected and the strongest signal. Quality values of 8 and 9 indicate errors during the depth analysis or beams without feasible returns. Finally a quality factor of 0 is assigned if the BDA indicates a

Table 1. Quality Flags Attached to the Data by the SEABEAM 1000 Electronic and the Corresponding Recording Software HSO

Quality Flag	Pattern	Detection Domain
0	unrealistic slope	space
1–4	$A_2 > A_1$	time/amplitude
5	$A_1 = A_2$	time/amplitude
6,7	$A_2 < A_1$	time/amplitude
8, 9	no echo, internal error	

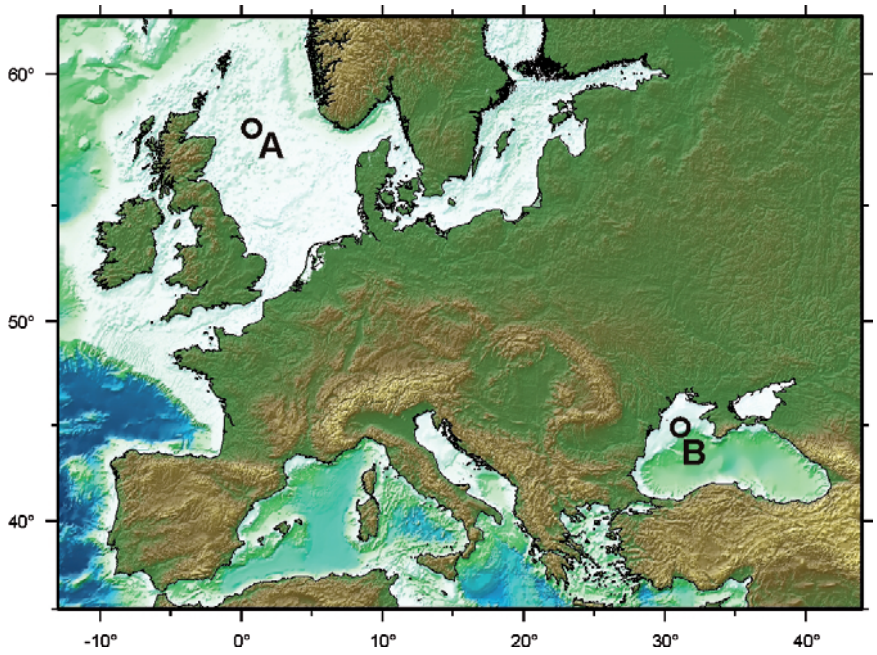

Figure 2. Locations of the working areas (A) in the North Sea (blow-out site) and the Dnepr shelf area in the Black Sea (B).

reliable seafloor signal but the slope to neighboring beams of the same swath is too steep.

3. Data Processing

[17] The data were processed applying correct sound velocity profiles and system corrections such as roll bias and exported to be visualized in Fledermaus in three dimensions. It is critical that ALL data are used, particularly those flagged with quality 0, 5, 6 and 7 by the system. Data points flagged with quality 0 (q0) are most likely to present bubbles. If there is a dense bubble cloud, the transmitted sound waves are strongly damped and bottom reflections become weak (q5, q6, q7).

[18] Standard postprocessing techniques, e.g., median or mean filtering, standard grid interpolation or the novel CUBE [*Calder and Mayer*, 2003] should be avoided. These postprocessing steps are well adapted for seafloor map generation but suppress water column data. Shallow-pass filter routines might be applied before 3-D presentation.

4. Field Data

4.1. Blow-Out Site, North Sea

[19] During a cruise with R/V *Alkor* (Alk 259, June 2005) we investigated a leaking gas well in the North Sea at about 95 m water depth (Figure 2). This site has been leaking since 1990 and was found to be active in 1996 [*Rehder et al.*, 1998] and during our studies in June 2005. Captured centimeter-sized gas bubbles at the sea surface showed a gas composition with more than 60% methane. Up-welling process could be identified due to turbulent mixing patterns in temperature and density profiles, which were measured during CTD-casts in the vicinity of the blow-out. Because of this, the blow-out site must be regarded rather as a gas plume than a gas flare. At the sea surface it caused a bubble patch of 30 m in diameter well visible from a greater distance. In Figures 3a and 3b, postprocessing (i.e., incorporation of bad flagged data) for finding free gas was applied. Well visible are data that form an almost vertical column with the highest data points at 7 m water depth. Color coded for the beam number (Figure 3a), it becomes obvious that with increasing distance to the seafloor the beams sequentially belong to the outer parts of the swath. At the same time, the data quality changes from bad data (red) to unrealistic slope data (yellow) for the highest data points (Figure 3b). The position where bubbles have been observed at the sea surface fits precisely with the topmost data points. This alone may prove that these data points are caused by bubbles; however, amplitude data show that these data points indeed

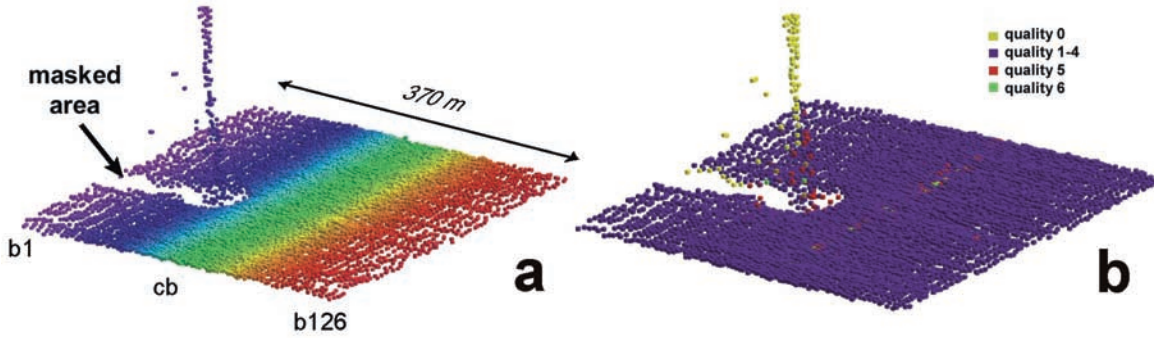

Figure 3. Multibeam data from the blow-out site of one single line (180 kHz, vertical exaggeration: 2.8). Figure 3a shows data color coded by beam number ranging from beam 1 (b1, portside) to beam 126 (b126, starboard side); cb is the center beam. Figure 3b shows the same data as Figure 3a but is color coded by quality.

have relatively high values, which can be expected from several millimeter to cm-sized bubbles. The bubble abundance is so high that they physically mask the seafloor to be reached by the transmitted pressure wave. The large number of data points with quality factor 0 (extreme slope) prove conventional and automatic data processing would have deleted most of the data indicative for bubbles.

[20] Knowing that the bad quality data high up in the water column are caused by reflections of bubbles in the bubble plume, it is possible to map the total dimension of the plume. This requires insonification of the area from many different directions and incident angles to account for the geometric masking effect. Figure 4 shows the compiled data set recorded from different incident angles of several survey lines. The grey colored seafloor was generated in a conventional way (excluding bad-flagged data and editing). The gridded data shows a circular depression, 50 m in diameter and 20 m around the actual drill hole. The depth-colored water column data are mainly caused by bad quality data similar to those shown in Figure 3b. It became clear that the gas release itself occurs in the morphologic depression. The dimension of the uppermost part of the acoustic plume correlates with visual observations of the 30 m-wide bubble patch at the sea surface (Figure 4).

4.2. Natural Methane Seepage, Black Sea

[21] We applied the same method to process data from a less intense seep area in about 220 m water depth in the Black Sea (Figure 2). Seep sites in this area have been reported by several authors during the last 10 years [*Egorov et al.*, 1998; *Michaelis et al.*, 2002; *Naudts et al.*, 2006]. The data presented were recovered on a research cruise with R/V *Poseidon* (317-3) in October 2004. One advantage of hydroacoustic studies in the Black Sea is that there are no "disturbing" signals caused by fish below 100 m water depth as the Black Sea becomes anoxic at this depth.

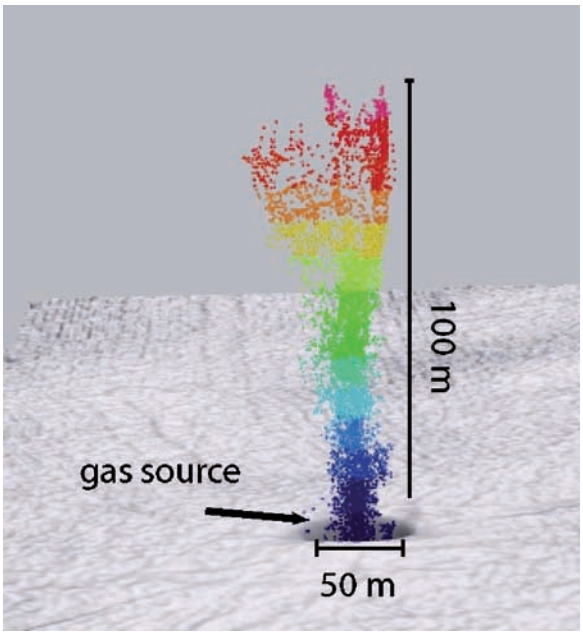

Figure 4. Data recorded during several survey lines covering the same location. The gray seafloor relief is generated in a conventional manner, whereas the depth colored soundings in the water column derive from "bad" data. The plume-forming bubbles could be detected by the multibeam system to rise up to 7 m below the sea surface. A 3-D movie of this data set is available as auxiliary material (Movie S1)[1].

[1]Auxiliary materials are available in the HTML. doi:10.1029/2007GC001577.

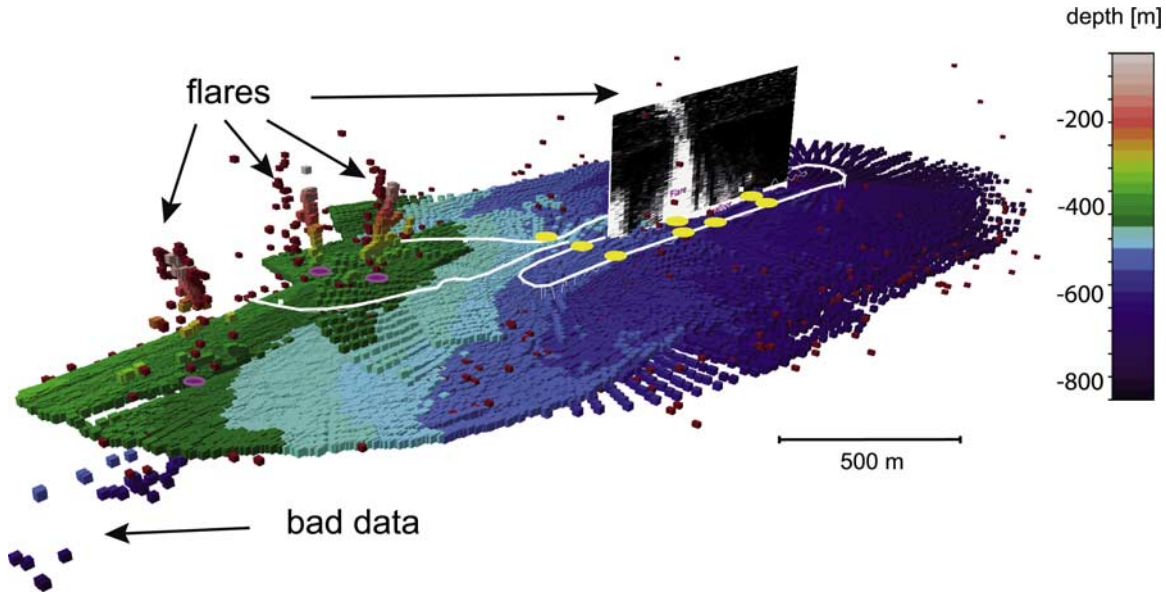

Figure 5. Multibeam depth data presentation of any quality from the Dnepr area in the Black Sea. Red dots are plotted with a small horizontal offset (for better visibility) presenting soundings flagged with quality 0. The ship track is plotted as a white line. Each flare detected in the center beam is drawn as a yellow circle (along-track), where the vertical image is a depicted echo time series from this center beam recorded as WCI. Flare positions detected by the submersible JAGO are shown as purple circles. A 3-D movie of part of this data set is available as auxiliary material (Movie S2).

[22] A reduced data set is visualized in Figure 5 in a similar way to Figure 4. Four possible flare sites could be identified. Their positions coincide with seep locations detected during submersible dives and WCI studies carried out during multibeam mapping (yellow and purple circles, respectively, in Figure 5). Again, mainly bad-flagged data contribute to the vertical excursions and might be interpreted simply as spikes of the bathymetric data.

[23] Although spikes are common in multibeam data, we are convinced that these bad-flagged data are reflections by bubbles for the following reasons:

[24] 1. Visual observation by submersible (Figure 5, purple circles) and WCI of the centre beam (Figure 5, yellow circles) provided ground truthing for several flares along the ship's track. Additional flares off the ship's track but inside the multibeam swath coverage are likely to occur.

[25] 2. Applying the same postprocessing technique for data from areas where no active seepage was found by visual or WCI studies, we did not find bad-flagged data positioned high in the water column.

[26] 3. The bad-flagged data systematically plot exceptionally high above the seafloor and resemble the shape of a flare.

[27] Comparing the WCI flare detection of the recorded centre beam (Figure 5, yellow ellipses) and the multibeam data, WCI provides proof of the occurrence of free gas. The great advantage of using multibeam data is the large coverage. The combination of both methods allows recognition and mapping of bubble release/flares of a large area parallel to normal multibeam mapping.

5. Summary and Conclusion

[28] We propose a processing procedure for finding gas flares in the water column with multibeam systems. This procedure makes use of the fact that the strong reflectivity of gas bubbles for acoustic waves leads to bubbles being misinterpreted as bottom reflections by the multibeam system. Depending on the system bottom detection algorithm, the strong reflections are recorded and might be flagged as bad or suspicious. During conventional multibeam postprocessing those data are typically not used for further processing. But

visualizing such bad flagged data in a raw data presentation is a very effective way for finding gas in the water column. Two data sets from sites where intense bubble release has been identified visually or by WCI show flare-shaped reflections caused by bubbles.

[29] The steered narrow beam of multibeam systems allows the exact determination of the echo origin and therefore allows exact positioning of the gas source at the seafloor. Seafloor masking due to strong backscatterers above the seafloor can be used as additional indication for bubbles. However, for 3-D mapping of bubble plumes the area has to be insonified from every direction. Doing this, a clear relation between the gas releasing spot and geological features such as pockmarks, ridges or (on a larger scale) mud volcanoes is possible. Huge amounts of multibeam data exist especially from the continental shelf and margin where gas escape is most likely to occur. Adapting the described processing and visualization procedure should be possible for, e.g., older ATLAS Hydrosweep and RESON data as these systems also record(ed) several quality values in each beam. Simrad systems eliminate suspicious data (bubbles) in real time (T. Eldevik, Kongsberg, personal communication, 2006). Thus former Simrad data sets are not very useful for gas detection in the water column. Reprocessing of data could be used for extensive flare imaging along continental margins for the detection of gas reservoirs deeper in the sediment supplying gas that migrates along geological pathways toward the seabed surface. At the same time this method can be used to detect leaking gas pipelines monitored by multibeam carrying AUVs.

Acknowledgments

[30] The authors would like to thank the German Government (BMBF) for supporting our research financially through a grant (COMET, 03G0600D) and the EU for supporting Jens Greinert with a Marie Curie Fellowship (MOIF-CT-2005-007436). Furthermore, we would like to thank Boris Schulze, Daniel Wendorff (L-3 Communications ELAC-Nautik GmbH) and Wilhelm Weinrebe (IFM-GEOMAR) for their great help with software support/adaptations and scientific input. Finally, we would like to thank the crew and the scientists who helped during the cruises with R/V *Poseidon* and R/V *Alkor*. This is publication GEOTECH - 254 of the R&D-Programme GEOTECHNOLOGIEN.

References

Calder, B. R., and L. A. Mayer (2003), Automatic processing of high-rate, high-density multibeam echosounder data, *Geochem. Geophys. Geosyst.*, *4*(6), 1048, doi:10.1029/2002GC000486.

Clay, C. S., and H. Medwin (1977), *Acoustical Oceanography: Principles and Applications*, 203 pp., Wiley-Interscience, Hoboken, N. J.

Clift, R., J. R. Grace, and M. E. Weber (1978), *Bubbles, Drops and Particles*, Elsevier, New York.

Egorov, V. N., U. Luth, C. Luth, and M. B. Gulin (1998), Gas seeps in the submarine Dnepr paleo-delta, Black Sea: Acoustic video and trawl data, *Ber. ZMK, Reihe E*, *14*, 11–22.

Greinert, J., and B. Nützel (2004), Hydroacoustic experiments to establish a method for the determination of methane bubble fluxes at cold seeps, *Geo. Mar. Lett.*, *24*, 75–85.

Greinert, J., Y. G. Artemov, V. Egorov, M. de Batist, and M. McGinnis (2006), 1300-m-high rising bubbles from mud volcanoes at 2080 m in the Black Sea: Hydroacoustic characteristics and temporal variability, *Earth Planet. Sci. Lett.*, *244*(1–2), 1–15.

Hovland, M., and A. G. Judd (1988), *Seabed Pockmarks and Seepages*, 293 pp., Springer, New York.

Judd, A. G., and M. Hovland (2007), Seabed Fluid Flow, 360 pp., Cambridge Univ. Press, New York, in press.

Judd, A. G., M. Hovland, L. I. Dimitrov, S. García Gil, and V. Jukes (2002), The geological methane budget at continental margins and its influence on climate change, *Geofluids*, *2*, 109–126.

L-3 Communications ELAC Nautik GmbH (2003), *Shallow and Medium Water Multibeam SEA BEAM 1000*, technical handbook, Kiel, Germany.

Leifer, I., and J. Boles (2005), Measurement of marine hydrocarbon seep flow through fractured rock and unconsolidated sediment, *Marine Pet. Geol.*, *22*, 551–568.

Lurton, X. (2002), *An Introduction to Underwater Acoustics: Principles and Application*, Springer, New York.

Mayer, L., Y. Li, and G. Melvin (2002), 3D visualization for pelagic fisheries research and assessment, *ICES J. Mar. Sci.*, *59*(1), 216–225.

McGinnis, D. F., J. Greinert, Y. Artemov, S. E. Beaubien, and A. Wüest (2006), Fate of rising methane bubbles in stratified waters: How much methane reaches the atmosphere?, *J. Geophys. Res.*, *111*, C09007, doi:10.1029/2005JC003183.

Michaelis, W., et al. (2002), Microbial reefs in the Black Sea fueled by anaerobic oxidation of methane, *Science*, *297*, 1013–1015.

Naudts, L., J. Greinert, Y. Artemov, P. Staelens, J. Poort, P. van Rensbergen, and M. de Batist (2006), Geological and morphological setting of 2778 methane seeps in the Dnepr paleo-delta, northwestern Black Sea, *Mar. Geol.*, *227*, 177–199.

Rehder, G., R. S. Keir, E. Suess, and T. Pohlmann (1998), The multiple sources and patterns of methane in North Sea waters, *Aquat. Geochem.*, *4*, 403–427.

Schmale, O., J. Greinert, and G. Rehder (2005), Methane emission from high-intensity marine gas seeps in the Black Sea into the atmosphere, *Geophys. Res. Lett.*, *32*, L07609, doi:10.1029/2004GL021138.